

Polariton Dispersion of Periodic Quantum Well Structures¹

A. V. Mintsev¹, L. V. Butov^{1,2}, C. Ell³, S. Mosor³, G. Khitrova³, and H. M. Gibbs³

¹ Institute of Solid State Physics, Russian Academy of Sciences, Chernogolovka, Moscow region, 142432 Russia

² Materials Sciences Division, E. O. Lawrence Berkeley National Laboratory, 94720 Berkeley, California, USA

³ Optical Sciences Center, University of Arizona, 85721 Tucson, Arizona, USA

Received October 24, 2002

We studied the polariton dispersion relations of a periodic quantum-well structure with a period in the vicinity of half the exciton resonance wavelength, i.e., the Bragg structure. We classified polariton modes using an approximation of a large number of quantum wells. The polariton effective masses are found to be very small and equal to 10^{-3} – 10^{-4} of the free-electron mass. © 2002 MAIK “Nauka/Interperiodica”.

PACS numbers: 73.21.Fg; 71.36.+c; 73.20.Mf

Semiconductor structures allow engineering of the light–matter interaction. The band structure and dispersion relation of the coupled mode of exciton and photon, called a polariton, can be controlled by the structure design, thereby opening great opportunities for fundamental studies of exciton and photon physics, as well as for device applications. Recently, considerable attention has been devoted to the study of photon–matter interaction in semiconductor microcavities (MCs) [1] and photonic band-gap materials [2], i.e., structures characterized by light-wavelength size. One of the advantages of polariton-dispersion engineering is the possibility to construct a bosonic quasiparticle with extremely small effective mass m . In particular, due to the small density of states in such a system, a statistically degenerate gas of polaritons may arise even at high temperatures and small densities (the temperature at which a quasi-2D gas of noninteracting bosonic quasiparticles becomes statistically degenerate is $T_0 = \pi\hbar^2 n / 2mk_B$ [3]).

In this paper, we consider the system of polaritons in a periodic quantum-well (PQW) structure with a period close to half the exciton resonance wavelength, i.e., in a Bragg structure. In PQW structures, due to the total confinement of excitons in QWs, the propagation of polaritons through the PQW is possible only because of the electromagnetic transfer of excitation through the barrier layers; in this sense, they are Wannier–Mott excitons for in-plane motion and Frenkel excitons for motion in the growth direction [4]. Before there were any experiments, several unique properties of polaritons in PQW structures had been predicted [4–9]. Ivchenko *et al.* [8] made two related and significant predictions. First, in an infinite Bragg structure with $d = \lambda/2$, the normal light wave is a standing wave characterized by two wave vectors $Q = \pm\pi/d$ with a field $E(z) \propto \sin(\pi z/d)$ with nodes at every QW position. This wave

does not couple to excitons, because the optical transition matrix element $\propto \int dz E(z)\Psi(z)$ is minimal and, therefore, Bragg PQW structures with a large number of QWs poorly emit and absorb resonant light in the normal direction [8]. Second, although it is a poor emitter, the Bragg structure is an excellent reflector: due to constructive interference between the light waves reflected by various QWs, the reflectivity of the Bragg structure is dramatically enhanced; in fact, in reflectivity or transmission, a set of N QWs with $d = \lambda/2$ is equivalent to a single QW (SQW) with a radiative coupling coefficient N amplified times over the value for an SQW [8].

The theoretical predictions initiated intense experimental studies. A strong amplification of the reflectance in Bragg PQW structures was observed in [10]. The enhancement of the signal decay rate in the Bragg structure was observed in the degenerate four-wave-mixing experiments in reflection geometry [11]. Recently, almost 100% reflectivity and the onset of a photonic band gap were observed in a Bragg PQW sample with $N = 100$ QWs [12]. These experiments confirmed that the constructive interference between the light waves reflected by various QWs can be treated as a huge ($\propto N$) enhancement of the radiative coupling coefficient [8]. Further resonant excitation studies revealed that the radiative coupling effects dominate not only the transmission, reflection, and absorption spectra but also the resonance Rayleigh scattering [13, 14].

In this paper, we study polariton-dispersion relations of high-quality Bragg and nearly Bragg PQW structures with $d \approx \lambda/2$. In our experiments, e–h pairs are generated by continuum absorption and lose energy by incoherent processes, populating low-energy carrier and polariton states. As shown in [12], under these conditions the PL spectra of a PQW structure cannot be explained by the radiatively uncoupled incoherent emission of 100 individual QWs but are dominated by

¹ This article was submitted by the authors in English.

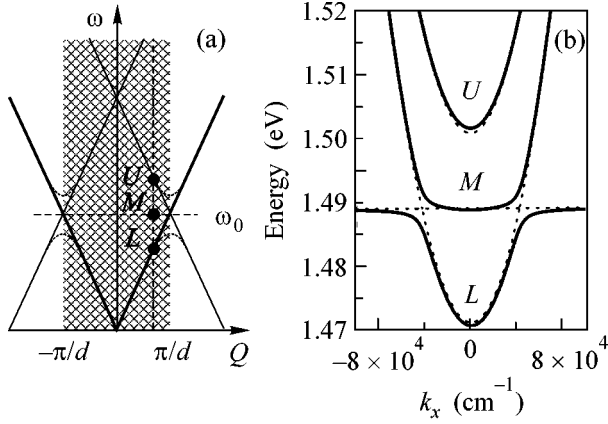


Fig. 1. (a) The scheme showing the dispersions of polaritons in PQW structures. In the infinite periodic structures, the polariton dispersions in the PQW growth direction (dotted lines) are constructed from the photon dispersions (bold lines), their replicas (thin lines), and exciton dispersion (dotted line). The polariton branches obey Eq. (2). The transition from an infinite to finite number of QWs, N , corresponds to the transition from continuous Q to discrete modes. For large N , the energies of the discrete modes (dots) fall on the continuous branch dispersions at $Q_j = \frac{\pi j}{dN}$,

$j = 1, \dots, N$ (vertical dashed line). (b) An example of in-plane dispersions of polariton mode branches calculated using Eq. (2). Dotted lines represent dispersions of the exciton and standing waves of light. The polariton mode dispersions (solid lines) are formed by anticrossing dispersions of the exciton and photon.

the cooperative emission from radiatively coupled QWs, i.e., by polaritonic states. Radiative coupling of the QWs occurs without any external coherent excitation.

The non-AR-coated PQW sample (DBR28) contains $N = 100$ 8.5-nm-thick $\text{In}_{0.04}\text{Ga}_{0.96}\text{As}$ QWs between GaAs barriers (for details, see [12]). The use of low-In-concentration QWs ensures that the background refractive indices of the well and barrier are nearly identical, thereby eliminating the photonic band gap arising from a distributed Bragg-mirror-like reflectivity. A decrease in flux with increasing radius during the growth on a rotating substrate provides an experimental way to continuously scan d . For cw PL studies, the excitation was provided either by an HeNe laser (excitation energy $\hbar\omega = 1.96$ eV) or by a Ti : sapphire laser. The excitation was focused to a 50- μm spot. Experiments were performed in a He_4 cryostat at $T = 1.5$ K.

The theoretical analysis of the polariton mode dispersion is based on the transfer-matrix approach that describes light propagation through a multilayer structure by solving the Maxwell wave equation including the corresponding boundary condition at each interface (LDT). According to [5, 9], the eigenmodes of the self-consistently coupled light-QW-exciton system in an infinite PQW structure obey the dispersion relation

$$\cos(Qd) = \cos(k_z d) - \frac{\Gamma_0 k/k_z}{\omega_0 - \omega - i\Gamma} \sin(k_z d), \quad (1)$$

where Q is the wave vector of light along the PQW growth direction reduced to the first Brillouin zone, $k = \omega/\hbar c$, $k_z = \sqrt{\epsilon_b k^2 - k_x^2}$, k_x is the in-plane polariton wave vector, ω_0 is the exciton resonance energy, and Γ_0 and Γ are, respectively, the radiative and nonradiative exciton damping constants in a single QW. As was shown in [9], for finite number N of QWs, the eigenmodes correspond to the discretized values of the complex wave vector Q . For large N , the values of wave vector tend to become real and equally spaced, and Eq. (1) transforms to

$$\cos(Q_j d) = \cos(k_z d) - \frac{\Gamma_0(\omega_0 - \omega)k/k_z}{(\omega_0 - \omega)^2 + \Gamma^2} \sin(k_z d), \quad (2)$$

where $Q_j = \frac{\pi j}{dN}$, $j = 1, \dots, N$. The roots of Eq. (2) $\omega = \omega(j, k_x)$ correspond to the eigenenergies of the polariton modes. The polariton energies also tend to become real for large N and, therefore, since the imaginary part of energies yields the radiative width of PQW polaritons, polariton states become stationary in the high- N limit, similar to bulk polaritons [7, 9].

The origin of polariton modes in PQW structures can be understood with the schemes shown in Fig. 1. Figure 1a schematically shows the dispersion of polaritons in the PQW growth direction. For infinite N , the polariton dispersions are constructed from the photon dispersions, their replicas, and exciton dispersion. We concentrate below on the energy region close to the exciton resonance. Around ω_0 , there are three PQW polariton branches originating from the folded photon dispersion and exciton dispersion: the upper (U), the middle (M), and the lower (L) one. The splitting between the branches at the anticrossing point at $Q = \pi/d$, proportional to the electromagnetic coupling between the photon and exciton, is small compared to ω_0 and is exaggerated in Fig. 1a. For finite and large N , the energies of the discrete modes fall on the continuous branch dispersions at the momenta $Q_j = \frac{\pi j}{dN}$, $j = 1,$

\dots, N for the j th polariton mode; i.e., the continuous branch and discrete modes obey Eq. (2) with the same r.h.s. We mark the upper j th mode as U_j and so on. Figure 1a presents the case of a Bragg structure with $d = \lambda/2$, i.e., with $\omega_0 = \pi c/d\sqrt{\epsilon_b}$; the modification of the scheme for different d is straightforward. An example of the in-plane dispersions for U , M , and L polariton branches is shown in Fig. 1b. The dispersions were calculated using Eq. (2) for $d/\lambda = 0.501$, $Q_j = 0.99\pi/d$, and $\Gamma_0 = 20 \mu\text{eV}$. The polariton modes are formed by the anticrossing dispersions of the exciton and standing waves of light (Fig. 1b). Note that the mode M_N is a

standing wave with a field $E(z) \propto \sin(\pi z/d)$ with nodes at every QW position $\forall d$ and $\forall k_x$, and its optical transition matrix element is zero.

Figure 2a shows the cw spectra of PL emitted in the direction normal to the PQW structure. Spectra are taken from different positions on the sample corresponding to different periods d , as labeled in Fig. 2a. Figures 2b and 2c present the measured PL energy and intensity of polariton modes at $k_x = 0$ corrected for the exciton energy shift due to a change in the QW thickness. The radiative mode splitting well exceeds the inhomogeneous exciton linewidth. The solid and dashed lines show positions of the eigenmodes at $k_x = 0$ calculated using Eq. (2). The best agreement between the experiment and Eq. (2) is achieved using $\Gamma_0 = 20 \mu\text{eV}$ (dashed lines). The linear fit to the HWHM of reflectivity spectrum vs. N gives $\Gamma_0 = 27 \mu\text{eV}$ [12]. The eigenmodes calculated using Eq. (2) with $\Gamma_0 = 27 \mu\text{eV}$ are also shown in Fig. 2b. All polariton modes observed in the experiment are clearly classified. This confirms that the QW number $N = 100$ is large enough to validate the approximation of Eq. (2) with real and equally spaced Q_j [9].² Figure 2c shows eigenmodes (solid lines), reflection dips (triangles), and absorption peaks (squares) calculated for $N = 100$ PQW using the Lorentzian excitonic susceptibility within an LDT approach [12]. Here, the absorption A is defined as $A = 1 - R - T$, where R is the reflection and T is the transmission. The best agreement between the experiment and the theory is achieved with $\Gamma_0 = 27 \mu\text{eV}$, in agreement with [12]. As expected, PL clearly follows the absorption; thus, the results of the LDT calculations are in good agreement with the experiment.

To measure the dispersion of the PQW polariton modes, we studied angularly resolved PL following experiments in [15], where this method was applied to study the dispersion of polaritons in MCs. The dispersions of polariton modes are revealed via their PL energy vs. $k_x = k \sin \phi$ dependence, where ϕ is the external angle between the emitted photon and the direction normal to the PQW structure. The measured dispersions of polariton modes are presented in Fig. 3. The dashed lines show positions of the eigenmodes calculated using Eq. (2). Dispersions of the polariton modes numerically calculated using LDT for 100 QWs (open squares) are in good agreement with the experimental data (Fig. 3). The calculation based on Eq. (2) has no fitting parameter and uses the value of Γ_0 obtained from the fit to the experimental data in Fig. 2. The main result of the polariton dispersion measurements is that the polariton effective masses are very small. In particular, for the mode M_{N-1} , $m \approx 5 \times 10^{-4} m_0$, they are close to the

² The calculation of the complex wave vectors Q by using the transfer matrix of a finite 100-QW structure [9] shows that there is a finite imaginary part for periods where the corresponding mode is bright. This implies that the large- N approximation is not validated over the whole range of periods.

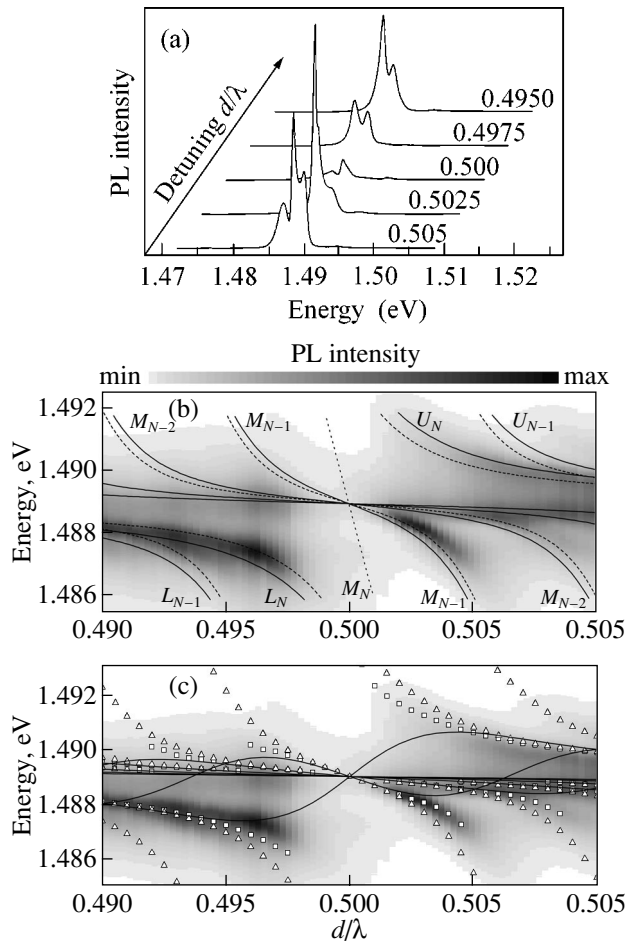


Fig. 2. (a) PL spectra in the normal direction in the reflection geometry for the non-AR-coated $N = 100$ $\text{In}_{0.04}\text{Ga}_{0.96}\text{As}/\text{GaAs}$ PQW structure under cw nonresonant excitation at 1.96 eV. Spectra are taken from different positions on the sample corresponding to different periods d ; $T = 1.5$ K. Poor emission in the normal direction at Bragg resonance, $d = \lambda/2$, reveals the vanishing overlap between the QW excitons and the standing wave of light. (b) The measured PL energy and intensity of polariton modes vs. d (grayscale map). The mode energies calculated using Eq. (2) with $\Gamma_0 = 20 \mu\text{eV}$ ($\Gamma_0 = 27 \mu\text{eV}$) are shown by dashed (solid) lines. The mode classification includes the branch U , M , or L index and the $j = 1, \dots, N$ number (Fig. 1). The optically inactive M_N mode is absent in the PL spectra. (c) Absorption peaks (squares), reflection dips (triangles), and eigenenergies (solid lines) calculated using LDT through a finite non-AR coated 100 QW structure. Note that the functional dependence of A on the period is different for an AR-coated structure.

effective mass of microcavity polaritons. This agreement is natural, because the polariton dispersions are determined by the anticrossing dispersions of an exciton and standing waves of light both for PQWs and MCs. Note that small density-of-states effective mass [$1/m = 2/\hbar^2 \partial E / \partial (k^2)$] is characteristic of most of the polariton modes (Fig. 3).

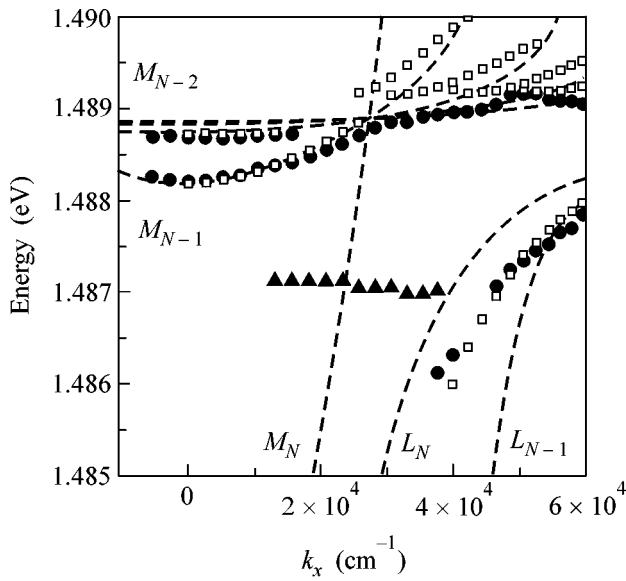


Fig. 3. Measured PL energy of polariton modes (solid points) in non-AR coated $N = 100$ $\text{In}_{0.04}\text{Ga}_{0.96}\text{As}/\text{GaAs}$ PQW structure with $d = 0.5025 \lambda$ vs. k_x under cw nonresonant excitation at 1.495 eV; $T = 1.5$ K. Triangles correspond presumably to the PL of localized states. The mode energies calculated using Eq. (2) with $\Gamma_0 = 20 \mu\text{eV}$ are shown by dashed lines. The polariton effective masses are extremely small; e.g., the quadratic fit to the mode M_{N-1} dispersion at small k_x yields $m \approx 5 \times 10^{-4} m_0$. The calculated absorption peaks using a Lorentzian excitonic susceptibility for the propagation through a 100-QW non-AR coated PQW structure with $\Gamma_0 = 27 \mu\text{eV}$ are shown by open squares.

We notice that the linewidth of the polariton PL from the $N = 100$ PQW sample is sometimes narrower than the linewidth of exciton PL from SQWs grown under as nearly as possible identical conditions. The smallest PL linewidth, ≈ 0.15 meV, observed in $N =$

100 PQW at $d \approx 0.5025 \lambda$ is ≈ 4 times narrower than the exciton PL linewidth in the SQWs. The effect of line narrowing due to the radiative coupling between the QWs clearly dominates over the broadening effects originating from the inhomogeneities of QW thickness, etc.

This work was supported by the Russian Foundation for Basic Research, INTAS (YSF no. 01/2-50), NSF AMOP, JSOP (AFOSR and ARO), and COEDIP.

REFERENCES

1. For a review, see G. Khitrova, H. M. Gibbs, F. Jahnke, *et al.*, *Rev. Mod. Phys.* **71**, 1591 (1999).
2. E. Yablonovitch, *Phys. Rev. Lett.* **58**, 2059 (1987).
3. A. L. Ivanov, P. B. Littlewood, and H. Haug, *Phys. Rev. B* **59**, 5032 (1999).
4. L. V. Keldysh, *Superlattices Microstruct.* **4**, 637 (1988).
5. E. L. Ivchenko, *Fiz. Tverd. Tela (St. Petersburg)* **33**, 2388 (1991) [*Sov. Phys. Solid State* **33**, 1344 (1991)].
6. L. C. Andreani, *Phys. Lett. A* **192**, 99 (1994).
7. D. S. Citrin, *Solid State Commun.* **89**, 139 (1994).
8. E. L. Ivchenko, A. I. Nesvizhskii, and S. Jorda, *Fiz. Tverd. Tela (St. Petersburg)* **36**, 2118 (1994) [*Phys. Solid State* **36**, 1156 (1994)].
9. L. C. Andreani, *Phys. Status Solidi B* **188**, 29 (1995).
10. V. P. Kochereshko, G. R. Pozina, E. I. Ivchenko, *et al.*, *Superlattices Microstruct.* **15**, 471 (1994).
11. M. Hübner, J. Kuhl, T. Stroucken, *et al.*, *Phys. Rev. Lett.* **76**, 4199 (1996).
12. M. Hübner, J. P. Prineas, C. Ell, *et al.*, *Phys. Rev. Lett.* **83**, 2841 (1999).
13. J. P. Prineas, J. Shah, B. Grote, *et al.*, *Phys. Rev. Lett.* **85**, 3041 (2000).
14. B. Grote, C. Ell, S. W. Koch, *et al.*, *Phys. Rev. B* **64**, 045330 (2001).
15. R. Houdre, C. Weisbuch, R. P. Stanley, *et al.*, *Phys. Rev. Lett.* **73**, 2043 (1994).